In Situ Observation of Droplet Nanofluidics for Yielding Low-Dimensional Nanomaterials

Zheng Fan, Jean-Luc Maurice, Ileana Florea, Wanghua Chen, Linwei Yu, Stéphane Guilet, Edmond Cambril, Xavier Lafosse, Laurent Couraud, Sophie Bouchoule, et al.

In Situ Observation of Droplet Nanofluidics for Yielding Low-Dimensional Nanomaterials

Zheng Fan[1*,#], Jean-Luc Maurice[1], Ileana Florea[1], Wanghua Chen[1,3], Linwei Yu[1,4], Stéphane Guilet[2], Edmond Cambril[2], Xavier Lafosse[2], Laurent Couraud[2], Sophie Bouchoule[2], Pere Roca i Cabarrocas[1]*

[1]Laboratoire de Physique des Interfaces et des Couches Minces, CNRS, École Polytechnique, Institut Polytechnique de Paris, 91128 Palaiseau, France

[2]Centre de Nanosciences et de Nanotechnologies, CNRS, Université Paris-Sud, Université Paris-Saclay, Avenue de la Vauve, 91120 Palaiseau, France

[3]School of Physical Science and Technology, Ningbo University, Ningbo 315211, China

[4]School of Electronic Science and Engineering, Nanjing University, 210096 Nanjing, China

*Emails: fanzheng@shanghaitech.edu.cn, pere.roca@polytechnique.edu

#Present address: Quantum Device Lab, Shanghaitech University, Shanghai 201210, China

Keywords: *in situ* transmission electron microscopy, self-propelled droplet transport, reactive wetting, low-dimensional nanomaterial, in-plane Si nanowire

Abstract: Droplet based micro/nanofluidics has been demonstrated as a versatile tool in a wide range of fields. In particular, seeded growth of planar low-dimensional nanomaterials often relies on crawling metal droplets as catalytic media where nucleation and crystal growth proceed. However, direct observations of nanomaterials growth led by self-propelled droplet transport remain rare, which leaves many open questions on droplet behavior during growth.

Here, we report *in situ* observations of in-plane Si nanowires growth in a transmission electron microscope, where an indium droplet migrates on a silicon nitride membrane coated by a layer of hydrogenated amorphous silicon (*a*-Si:H), dissolves the *a*-Si:H coating film on the membrane, and results in the production of a crystalline Si nanowire in its trail. This *in situ* observation, combined with the geometric investigation of the nanowires, presents nice consistency with de Gennes' theoretic prediction of reactive wetting induced droplet motion. Interestingly, we recorded a nanoflake-to-nanowire transition when the growth rate was increased by heating the membrane from 350 °C to 400 °C. This work directly unveils rich transport mechanism of catalytic droplets, which is expected to be a new platform for producing diverse low-dimensional nanomaterials and promote their potential applications in nanoscience and technologies.

1. Introduction

Droplet transport exhibits powerful potential in various applications like material synthesis, water collection, electronics cooling, electricity generation and biotechnologies.[1-10] Regarding low-dimensional nanomaterials growth, metal droplets are often used to mediate nucleation and crystal growth, which dates back to Wagner's pioneering work on gold catalyzed Si whiskers growth via vapor-liquid-solid (VLS) process.[11-13] Moreover, surface running metal droplets have been exploited to enable direct writing of in-plane nanomaterials, which opens novel avenues for realizing mixed-dimensional heterostructures.[14] Substantial efforts have been made on the programmable manipulation of crawling catalytic droplets on substrate surfaces. For example, a wide group of metal droplets can be trapped along nanofacets,[15-18] guiding steps,[19, 20] or nanochannels,[21] which facilitates the self-assembly of horizontal CNTs,[15] Si,[16],[19],[21] III-V,[17] III-N nanowires (NWs),[18] and Si/Ge island chains.[20] Moreover, gold droplets are reported to

lead the growth of horizontal Ge nanocrawlers on graphene surface, thus realizing 1D/2D heterostructures.[22] Recently, VLS-grown MoS_2 nanoribbons have been realized by moving Na-Mo-O droplets, which avoids dry etching process to pattern the 2D sheets.[12] In a reversal manner, nickel droplets can migrate on graphene sheets in H_2 atmosphere and etch them into nanoribbons having a width below 10 nm.[23] As a matter of fact, such self-propelled droplet transport can be associated with a large family of micro/nanofluidic phenomena based on wettability gradient induced droplet surface migration, where videos were recorded as direct evidences.[24-30]

However, when droplets shrink down to nanometer scale, *in situ* transmission electron microscopy (TEM) is regarded as a powerful tool, as it can directly reveal details about events of nucleation and crystal growth, as well as kinetics at interfaces between catalysts and nanocrystals.[31-38] However, direct observation is still in high demand for the low-dimensional nanomaterials growth mediated by crawling nanodroplets, where the droplet transport behavior and the droplet-crystal interfaces highly determine the final nanostructures.[20],[40] To this aim, we select indium (In) droplets catalyzed in-plane solid-liquid-solid (IPSLS) Si NWs as a platform,[39] to explore the dynamics of catalytic droplet transport by *in situ* TEM technique.

2. Experiments

***In situ* TEM experiment**: we used Aduro Thermal E-chips (Protochips Incorporated) for the *in situ* TEM observation of in-plane solid-liquid-solid growth. They consisted in a ~50 nm thick amorphous SiN_x membrane laying on a heating silicon carbide (SiC) membrane that contains 7x7 holes in diameter of 7 μm. The growth was observed over the holes where there was only the SiN_x membrane. The temperature can be tuned continuously from room temperature to 1200 °C, based on Joule heating effect of the (doped) SiC by electrical current.

An In thin film of ~200 nm (in shape of discontinuous islands) was deposited on the E-chip by thermal evaporation (see Figure S2a in the Supplementary Materials (SM)). In order to decrease the density of In islands, the E-chip was dipped in 3% HCL solution for 3 minutes. After a ~1 min rinse in deionized (DI) water, the E-chip was placed on a hot plaque at 125 °C for 2 minutes to evaporate the DI water on it, as shown in Figure S2b. Then the E-chip was transferred to the 13.56 MHz RF-PECVD reactor, and treated by a standard H_2 plasma exposure for 5 minnutes (100 sccm of H_2, 400 mTorr, RF-power density of 62 mW cm^{-2} at substrate temperature of 300 °C). Figure S2c shows an SEM image of a membrane after H_2 plasma treatment, whose shapes evolved from irregular islands to spherical particles. After this SEM observation, the chip was returned to the PECVD system, and treated by: (a) a standard H_2 plasma exposure for 5 minutes; (b) 16 nm *a*-Si:H coating by standard deposition condition (5 sccm of pure SiH_4, 120 mTorr, RF power density of 24 mW cm^{-2} at substrate temperature of 150 °C). Then, the E-chip was quickly transferred to TEM equipment (JEOL-2010F field emission electron microscope). The silicon nanowire growth was activated via the following process: small In droplets (up to several hundred nm) leaked from large In droplets (up to several μm), migrated on *a*-Si:H coated SiN_x membrane and produced silicon nanowires, as shown in Figure S3.

STEM-HAADF EDX analysis: chemical analyses was performed in STEM-HAADF (scanning transmission electron microscope high-angle annular dark field) imaging mode of a 200kV Titan-Themis TEM/STEM electron microscope equipped with a Cs probe corrector and a ChemiSTEM Super-X detector. Prior to the analysis, FIB technique was used for the preparation of a cross-section lamella containing a Si NW inside the trench. The STEM-HAADF EDX chemical mapping was performed by considering the following elements of interest: the silicon Kα-1.73 keV ionization present also in the substrate and in the thermal oxide layer, the oxygen Kα-0.523 keV ionization edge coming also from the thermal oxide

layer and the carbon Kα-0.277 keV ionization edge from the protective layer. Figure S5 shows the SEM image illustrating the area containing a Si NW inside the trench for the lamella preparation.

Geometric studies of in-plane solid-liquid-solid Si NWs: The substrates for Si NWs growth were *c*-Si wafers with a 100 nm thermal oxide layer where In pads in size of 500 nm x 500 nm were defined by electron beam lithography and thermal evaporation. The nominal thickness of the pads was 5 nm or 50 nm. Then, the samples were transferred to the RF-PECVD reactor, and treated by a standard process for the Si NWs growth: (a) H_2 plasma treatment for 5 minutes to reduce the indium surface oxide at 300 °C; (b) *a*-Si:H deposition in three different thicknesses of 9, 19 nm (on 5 nm In pads) and 30 nm (on 50 nm In pads) at 150 °C. The *a*-Si:H thickness was calibrated by UV-vis spectroscopic ellipsometry (Jobin Yvon-MWR). (c) Annealing the sample at 450 °C in H_2 atmosphere (200 sccm, 1.9 Torr) for 10 minutes. We selected several successfully grown in-plane silicon nanowires from the samples for SEM (Hitachi S4800) observation. It has to be mentioned that, although the growth temperature in the RF-PECVD reactor cannot be compared with that on the TEM heating membrane, however 450 °C in RF-PECVD is a well optimized standard growth temperature that enable us to obtain Si NWs and statistically analyze their geometries.

The variation of In NP diameters was caused by the coalescence of NPs at the initial stage of nanowire growth. Figure S1a shows an IPSLS Si NW grown from a 5 nm In pad. As seen in Figure S1b, the as-evaporated In pad was a discontinuous film with In NPs smaller than 80 nm. As a matter of fact, not all the In NPs were able to dissolve the *a*-Si:H coating layer and thereafter produce Si NWs, most of them were sieged by the *a*-Si:H shells, which was probably made of Si. The discussion of the shell formation is detailed in Section 3 in SM. Once a droplet broke its shell and initiated the NW growth (see the starting point), it could "rescue" and accumulate other In NPs in its movement path by breaking their shells. Thereafter, the final droplet got a much larger size (~160 nm) and was released from the In

pad for NW growth (as seen in Figure S1c). Thanks to this irregular coalescence, we managed to obtained different sizes of In droplets migrating on the *a*-Si:H for the Si NWs growth. In addition, as 32 nm *a*-Si:H was too thick for NPs of 5 nm In pads to produce silicon nanowires, we chose 50 nm In pads instead.

3. Results and Discussion

Figure 1a shows an IPSLS Si NW grown at 400 °C on an amorphous silicon nitride (SiN_x) membrane coated with 40 nm of *a*-Si:H. A solid In nanoparticle (NP) can be observed at its end. Note that this observation took place at room temperature (RT). The selective area (red dashed circle) electron diffraction pattern (see the inset image) shows a [110] orientation at the NW front. Once the membrane was heated to 350 °C, a rich interplay between the In droplet, the *a*-Si:H coated membrane and the Si NW arose. Figure 1b displays a sequence of TEM images extracted from Video S1. The In droplet started to melt and dissolve the *a*-Si:H layer at *t*=2 s. The thin In thin film along the front edge of the droplet, in contrast with the thick droplet bulk, first advanced laterally into two wings from *t*=4 to 6 s, then straight away in the middle of the liquid-solid (LS) contact line at *t*=8 s, during which new phases of *c*-Si kept being precipitated (see the red part of the NW). One can observe that the moving droplet was held by two arms (marked by the two yellow dashed circles) until *t*=8 s, so the droplet wings were drastically stretched. However, the droplet managed to escape from the arms (probably the *c*-Si precipitates during the In droplet solidification, see Figure S5 in the SI) with its wings rapidly relaxing from *t*=10 to 14 s, meanwhile dissolving the *a*-Si:H along its relaxation path (see the red arrows), uncovering the footprint of the droplet's trail, whose borders are marked by the black dashed lines (we name it trench as seen in **Figure 3**a), and producing a new segment of NW with three facets in contact with the droplet (see the yellow part of the NW).

Regarding this IPSLS growth process from the angle of droplet motion, a wettability gradient on a solid surface is required, where unbalanced Young's force F_d drives a droplet moving towards a more wettable area.[24] This can be expressed by

$$F_d = \gamma_{LV}(cos\theta_b - cos\theta_a), \quad (1)$$

where γ_{LV} denotes the droplet surface tension, $\theta_{a,b}$ denote the equilibrium liquid-solid (L-S) contact angles at the receding and advancing sides of the droplet, respectively.

As no thin wetting layers were observed between the droplet and the *c*-Si NW, this shape evolution of the moving In droplet provides direct evidence that the enhancement of substrate surface wettability is due to the reactions between In and *a*-Si:H layer.[25] On the one hand, due to its random structure with a large number of defects,[39] *a*-Si:H may have an excess surface energy compared with *c*-Si (1.2 J m^{-2}),[42] which thereby should be also higher than those of SiO_2 and SiN_x (~50 mJ m^{-2});[43] on the other hand, the LS contact enables a reactive process of metal-induced crystallization (MIC) of *a*-Si:H.[45]

Moreover, the instabilities of the moving droplet were also recorded. The droplet-NW interface gradually developed three facets at *t*=14 s. By superposing the blue, red and yellow parts of the NW at *t*=14 s in the following TEM images, one can see that *c*-Si mainly precipitated normal to facet 2 at *t*=15 s, which brought about a risk of squeezing the droplet into two. Afterward, facets 1 and 3 did move forward until *t*=20 s, causing a remarkable elongation of the droplet-NW contact line that finally transferred to the irregular morphology of a faceted NW. Hereafter, the right wingtip of the droplet was pinched off so that the droplet relaxed and accumulated on the left side (*t*=21 to 22 s). This phenomenon occurred a second time later, where the faceted droplet-NW interface (see *t*=50 s) finally led to a growth of a *c*-Si nanoflake (NF, red part) rather than NW (blue part), as seen in Figure 1c. More detailed TEM analysis of the zigzag nanowire with the selected area electron diffraction patterns are

seen in Figure S13. Interestingly, the droplet broke up twice during its motion, at t= 21 s and 72 s, with the formation of tiny satellite droplets along its moving path. Such a phenomenon also occurs in an IPSLS process with Sn as catalyst, during which the Sn droplet keeps losing its mass which consequently results in the formation of tail-like Si or Ge nanowires. [49,50] This droplet break-up behavior is regarded as a ubiquitous signature during the deformation of the flowing viscous droplets, which could be attributed to the competition between the shearing force within the droplet and the droplet surface tension. [51, 52]

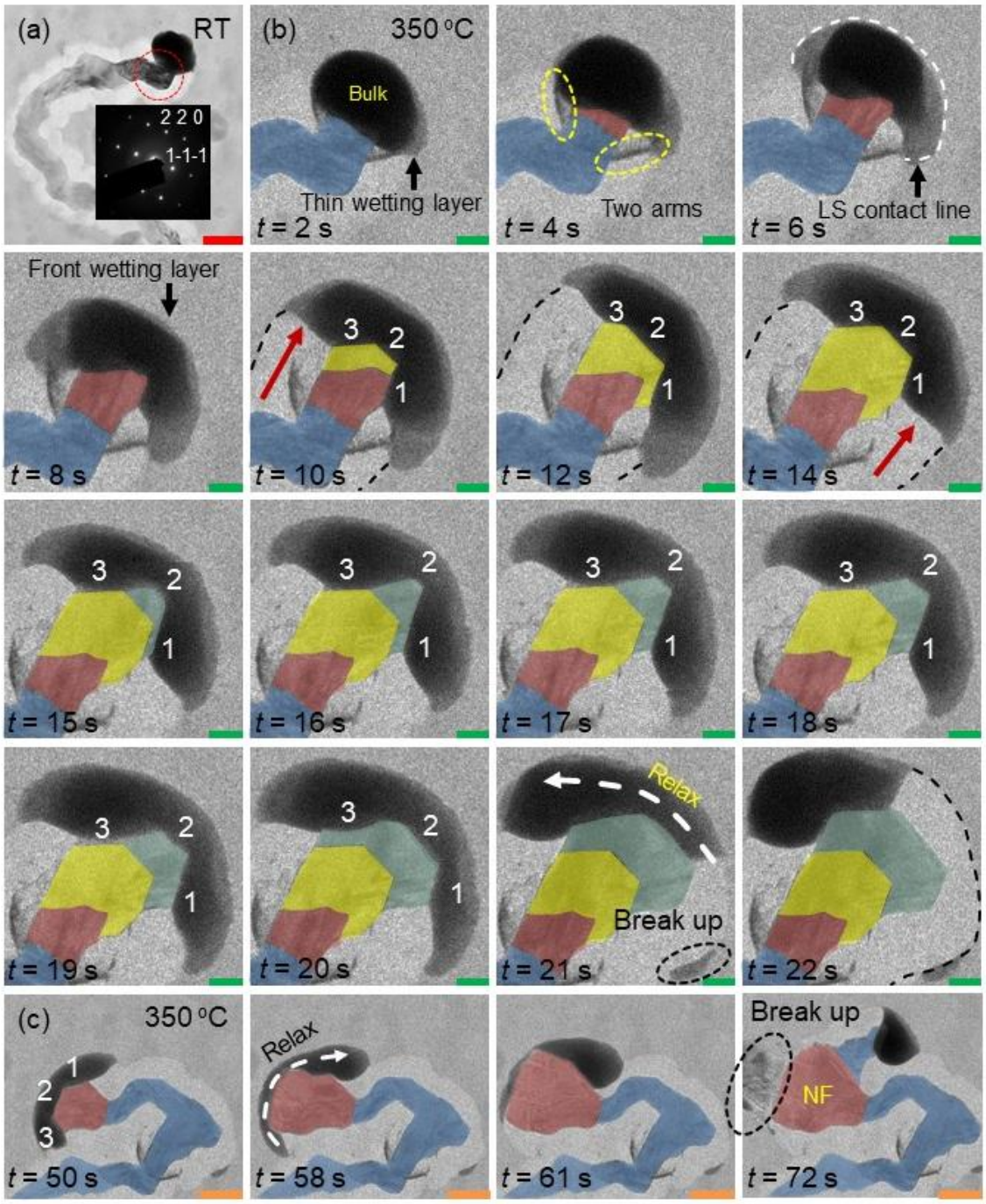

Figure 1. *In situ* TEM observation of an IPSLS Si NW growth at 350 °C. (a) TEM image taken at room temperature of a Si NW grown on a SiN_x membrane at 400 °C. Inset: selected area electron diffraction pattern in [1-12] zone showing the local orientation of *c*-Si. Two sequences of TEM images extracted from the growth of a NW at 350 °C (Video S1): (b) shows the reactive wetting of *a*-Si:H coated membrane by a deformed In droplet (from *t*=2 to 14 s), and the growth of NW in irregular morphology due to the faceted droplet-NW interface

(from *t*=15 to 22 s), with the droplet break up at *t*= 21 s; (c) a growth of *c*-Si NF rather than NW that results from the extensive stretching of In droplet along the faceted droplet-NW interface, with the droplet break up at *t*= 72 s. The scale bars are 200 nm, 100 nm, 400 nm in (a), (b) and (c), respectively.

Surprisingly, when lowering the temperature to 300 °C, the droplet steadily sat on the membrane, with a wetting layer along the LS contact line while no *c*-Si precipitated (see **Figure 2**a, *t*=0 s archived in Video S2). No significant In wetting behavior was observed in the trench (contoured by the black dashed line) nor on the NW. After ramping the temperature to 400 °C, the droplet spread into a fan-like shape and its migration kicked off (see Figure 2b). In contrast with the observation at 350 °C, the droplet's shape and the droplet-NW interface were fairly maintained, so the variation of NW diameter was eliminated to the largest extent. However, the droplet's moving direction changed frequently (e.g. from *t*=19 s to 23 s). This may be associated with the asymmetric wetting profile which could be attributed to some chemical inhomogeneity in the *a*-Si:H layer, where the droplet spread to the more wettable surface.[27] An interesting case of droplet turning (see Figure 2c) occurred once the In droplet was trapped in a situation where *a*-Si:H was only present to its right side (*t* =45 s), it spread and turned towards the *a*-Si:H covered surface (*t*=46, 47 s), which ensured that once the droplet touched the trench border (black dashed line), it left away. This self-avoiding of its moving trace is a significant feature of the droplet motion maintained by progressive reactive wetting, since once the droplet passes by and reacts with the solid surface, the solid surface energy will be lowered and will be unable to attract the droplet anymore.[25]

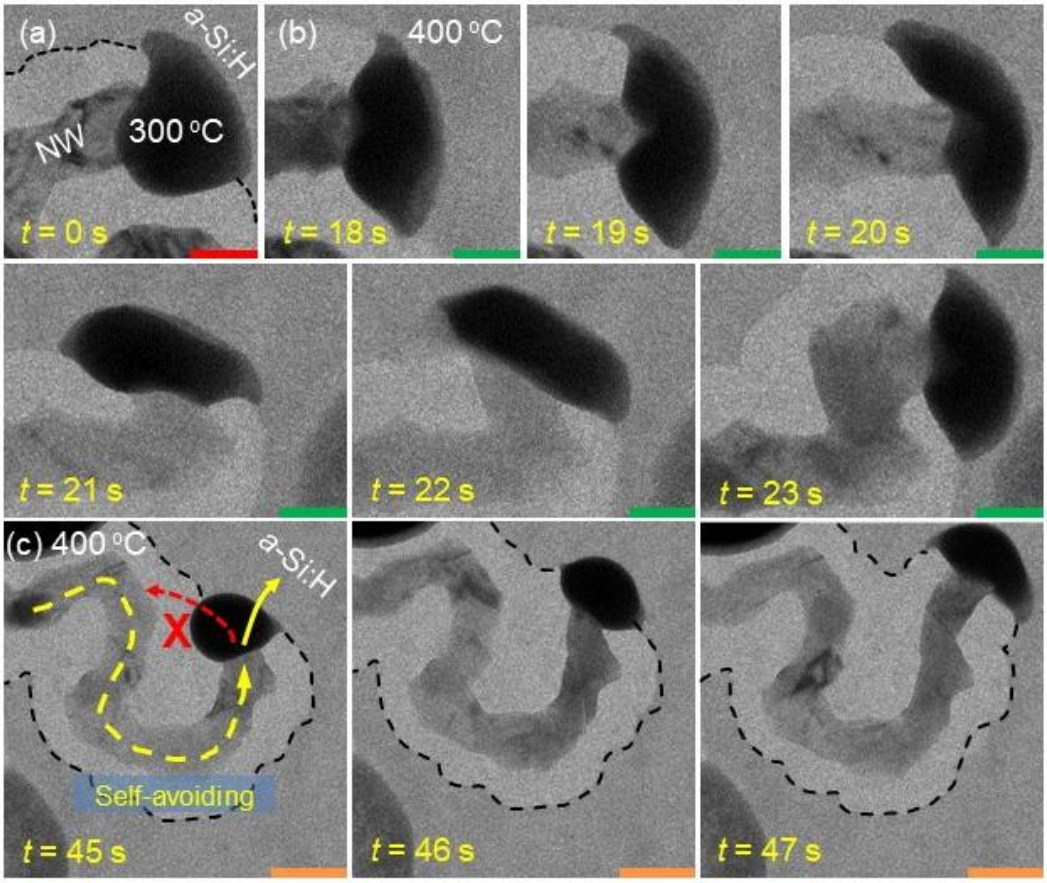

Figure 2. *In situ* TEM observation of an IPSLS Si NW growth at 400 °C. (a) In droplet steadily sat on the membrane at 300°C, with a thin wetting layer on *a*-Si:H. Two sequences of TEM images extracted from Video S2 are presented: (b) when the temperature reached 400°C, the droplet reactively wet the *a*-Si:H coated membrane surface and started to move randomly while producing a NW with a relatively uniform diameter; (c) droplet self-avoiding its trace: once touching the trench border, the droplet left away. The black dashed lines in (a) and (c) represent the trench boundaries. The scale bars are 150 nm in (a), (b) and 500 nm in (c).

Comparing the *in situ* observation at 350 °C with that at 400 °C, we find a growth variation from nanoflake to NW with increasing temperature, where the In catalyst evolved from a slow and drastically deformed droplet (～20 nm s^{-1}) to that in a fast (～100 nm s^{-1}) stick-slip motion [25]. Such a flake-to-fiber transition ubiquitously exists in the solidification

of Al-Si eutectic alloys, where the morphologies of Si crystals evolve from flakes to fibers with increasing growth rate.[46] Apparently, the lower temperature retards (at 350 °C, see Figure 1b, c) or even suppresses (at 300 °C, see Figure 2a) the Si diffusion into the In droplet and the following Si nucleation, which decelerates the droplet motion. However, the temperature dependent droplet reactive wetting needs to be elucidated, which predominantly affects the morphologies of the Si precipitates. Since the droplet surface tension varies little in such a narrow temperature window [44] (detailed calculation is seen in SM Section 1), the chemical reaction at the L-S (i.e. droplet-*a*-Si:H) interface should be accounted. In order to activate the Si heterogeneous nucleation from In droplet, the Si chemical potential difference between the supersaturated and saturated In droplet $\Delta\mu$ should overcome the nucleation barrier ΔG^*_{hetero}:

$$\Delta\mu_{Si} > \Delta G^*_{hetero}. \quad (2)$$

Being a process of heterogeneous nucleation from solution [43], Equation (2) can be transformed into (a more detailed deduction is provided in the SM Section 2)

$$C_{s,Si(In)} > C_{0,Si(In)} \exp\left[\sqrt[3]{\chi f(\theta_{Si-Sub})}\Omega_{Si}\gamma_{Si-In}/(k_B T)\right], \quad (3)$$

where $C_{s,Si(In)}$ and $C_{0,Si(In)}$ denote the Si concentration in the In droplet in a supersaturated state and in the equilibrium state, respectively, and $C_{0,Si(In)}$ can be considered as a constant from 350 °C to 400 °C [53]; χ the shape factor of the Si nucleus, Ω_{Si} the volume of a Si atom, $\gamma_{Si\text{-}In}$ the interfacial energy between the Si nucleus and the liquid In, k_B the Boltzmann constant, T the growth temperature, $f(\theta_{Si\text{-}Sub})$ the contact angle ($\theta_{Si\text{-}Sub}$) factor between the Si nucleus and the substrate, which increases monotonically with the increment of $\theta_{Si\text{-}Sub}$ [45]. Thereby, once the growth temperature T decreases, the droplet reactive wetting tends to evolve in two main aspects: on the one hand, before each step forward, the In droplet has to spread more aggressively to cover more *a*-Si:H area and feed itself more Si atoms, so that $C_{s,Si(In)}$ will be raised and a higher Si supersaturation degree (i.e. $C_{s,Si(In)}/C_{0,Si(In)}$) will be approached to

overcome the nucleation barrier ΔG^*_{hetero}, which consequently renders the formation of the multi-faceted droplet-NW interfaces; on the other hand, the Si nucleus tends to wet the substrate so that $f(\theta_{Si\text{-}Sub})$ will drop to compensate the lowered T, which gives rise to the growth of the flattened *c*-Si (that we name nanoflake) rather the cylindrical NW (see Figure 3b).

Furthermore, Equation (3) also brings insights to the zigzag growth of IPSLS Si (or Ge) nanowires catalyzed by Sn droplets [47,48]. Due to the higher equilibrium concentration (i.e. solubility) of Si (or Ge) in Sn compared with those in In (i.e. $C_{0,Si(Sn)} > C_{0,Si(In)}$, $C_{0,Ge(Sn)} > C_{0,Si(In)}$) [54,55], the Sn droplet has to intensify its spreading to accommodate more Si (or Ge) atoms to approach a higher critical supersaturation $C_{s,Si(Sn)}$ (or $C_{s,Ge(Sn)}$) for the nucleation. This is very similar to the growth of In catalyzed IPSLS Si NW at 350 °C, which favors the formation of the multi-faceted droplet-NW interfaces that renders higher probability of NW self-turning and the droplet mass loss along its trajectory.

Besides *in situ* TEM observations, we carried out a geometric analysis of IPSLS Si NWs, which provides additional information of the In droplet reactive wetting behavior. **Figure 3**a shows a scanning electron microscope (SEM) image of a typical IPSLS Si NW grown on SiO_2, with a solidified In nanoparticle (NP) and a trench that records the trace of In droplet migration. Direct evidence on the trench structure was obtained by performing high-angle-annular-dark-field scanning transmission electron microscopy (HAADF-STEM) energy-dispersive X-ray spectroscopy (EDX) chemical map on a cross-section of the NW TEM lamella prepared by focused ion beam (FIB), as seen in Figure 3b. The boundaries of *a*-Si:H layer (h_{aSi} denotes the thickness) are marked by a white dashed line. One can see that the NW is located at the trench center with *a*-Si:H completely exhausted, while a small amount of residual *a*-Si:H remains at the edges of the trench. A top-view scheme of a NW is illustrated

in Figure 3c, labeled with geometric parameters of the SLS system: d_{NP} represents the solid In NP diameter; d_{NW} represents the NW diameter; $d_{In\text{-}aSi}$ represents the trench width, which can be considered as the LS contact width.

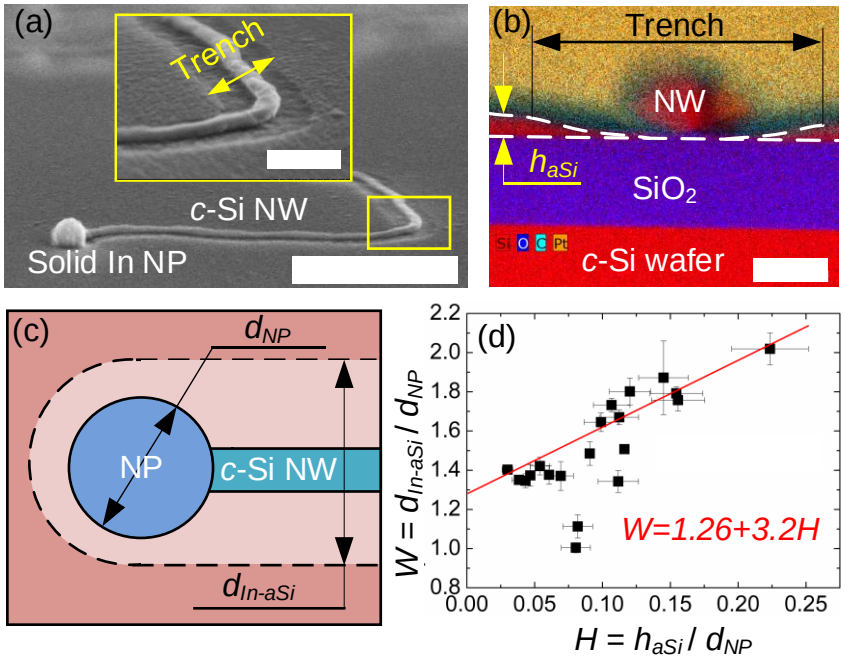

Figure 3. Geometric investigation of the IPSLS Si NW systems. (a) SEM image of an IPSLS Si NW grown on SiO_2. The inset image provides a closer view of NW located in the center of the trench. (b) HAADF-STEM EDX relative map of the cross-sectional profile of a NW at the center of the trench. h_{aSi} represents the *a*-Si:H thickness. (c) Top-view scheme of an IPSLS Si NW: d_{NW} represents the NW diameter, and d_{NP} is the solid NP size, $d_{In\text{-}aSi}$ is the trench width. (d) Geometric analysis shows $d_{In\text{-}aSi}/d_{NP}$ has a linear relationship with h_{aSi}/d_{NP}. The scale bars in (a), inset of (a) and (b) are 1 μm, 200 nm and 80 nm, respectively

We measured d_{NP} and h_{aSi} for Si NWs grown at 450°C in a plasma enhanced chemical vapor deposition (PECVD) reactor (see Experimental Section). At a given growth temperature, considering (d_{NP}, h_{aSi}) as the *input* parameters to a SLS system, (d_{NW}, $d_{In\text{-}aSi}$) can be viewed as the *output*. As the trench records the LS contact during droplet migration, this relationship can be given by

$$d_{In-aSi} = f(h_{aSi}, d_{NP}). \quad (4)$$

By transforming Equation (4) into

$$d_{In-aSi}/d_{NP} = g(h_{aSi}/d_{NP}, 1), \quad (5)$$

Figure 3d provides a linear fitting of this relationship:

$$\beta = 1.26 + 3.2\alpha, \quad (6)$$

where α denotes h_{aSi}/d_{NP}, and β denotes $d_{In\text{-}aSi}/d_{NP}$. The intercept of 1.26 indicates that if there is no *a*-Si:H coating layer (i.e. α approaches 0), β equals 1.26 (i.e. $d_{In\text{-}SiO2}$=1.26$d_{s\text{-}NP}$). Considering a constant mass of a spherical NP before and after melting, this ratio implies that an In droplet on a bare SiO_2 surface is a semi-sphere, with a contact angle θ_{SiO2} of 90°.[45] However, once the SiO_2 surface is coated by a thin film of *a*-Si:H, the L-S contact line is stretched in width (i.e. $d_{In\text{-}aSi} > d_{In\text{-}SiO2}$), therefore the contact angle shall be lowered (i.e. θ_{aSi} <90°), which fairly demonstrates that *a*-Si:H coating layer is *indium-philic*. Moreover, since β increases monotonically with increasing α, Equation (6) indicates that relatively thicker *a*-Si:H renders stronger droplet reactive wetting (i.e. the relative trench width β is broader on relatively thicker *a*-Si:H coated substrate). Considering a droplet with a constant volume at constant pressure and temperature, the thicker the *a*-Si:H coating layer is, the more Si atoms the droplet has to dissolve in order to deplete the *a*-Si:H beneath it for the *c*-Si precipitation (see Figure 3b). The Gibbs free energy change of the droplet (more precisely the liquid In-Si alloy) ΔG_{drop} is expressed as [56]

$$\Delta G_{drop} = \mu_{In}\Delta n_{In} + \mu_{Si}\Delta n_{Si}, \quad (7)$$

where $\mu_{In,Si}$ denotes the chemical potential of In and Si, respectively; $\Delta n_{In,Si}$ denotes the molar mass change of In and Si, respectively. Thereby, once the *a*-Si:H gets thicker, the droplet will have an excess Gibbs free energy contributed by the increment of Δn_{si}, which will render the droplet flattening to increase its surface free energy for approaching to a new equilibrium state, that is, the droplet spreading will be enhanced.

Combining our *in situ* TEM observations with the geometric analysis, we propose the following IPSLS growth mechanism. As illustrated in **Figure 4**a, an In NP evolves from solid to liquid on a SiO_2 substrate upon heating; and its non-reactive wetting on bare SiO_2 shifts to become a reactive mode once the SiO_2 surface chemistry is modified by adding an *a*-Si:H layer. Furthermore, a continuous NW growth led by a crawling droplet is mainly enabled by three cyclic events as seen in Figure 4b: (i) In droplet reactively wets *a*-Si:H based on a solid-liquid-solid process where liquid In alloys with Si atoms by dissolving *a*-Si:H until Si supersaturation, which thereafter activates heterogeneous nucleation and *c*-Si growth. Such process is driven by the Gibbs free energy difference between *a*-Si:H and *c*-Si;[48] (ii) consequently, a wettability gradient is established, from the non-reactive bare substrate (i.e. SiO_2, Si_3N_4, etc.) with precipitated *c*-Si to the surface coated by reactive *a*-Si:H; (iii) In droplet moves to the *a*-Si:H surface with higher wettability, which thereby maintains the droplet contact with *a*-Si:H. However, a *c*-Si NW is not the only type of product of a crawling droplet. As seen in Figure S4, for large size drops in micrometer scale, as there will be more sites for the silicon precipitation in such cases, separated Si crystals will be produced rather than a NW. Furthermore, our visualization of the reactive wetting induced droplet motion also brings deep insights into the VLS growth process in many aspects, which affects the NW tapering [57-59] and determine the VLS growth of lateral NWs [21, 60] (see Figures S7-S11).

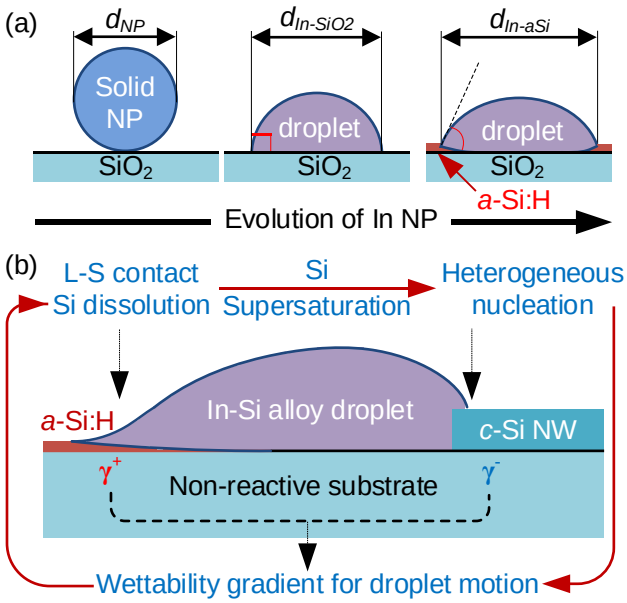

Figure 4. Mechanism of In droplet crawling on *a*-Si:H coated substrate for in-plane Si NW growth. (a) Evolution of an In NP from solid to liquid phase, from non-reactive spreading on bare SiO_2 to reactive spreading on *a*-Si:H coated SiO_2. (b) From side view, (i) In droplet reactively spreads and dissolves *a*-Si:H (high γ^+ surface), followed by the formation of In-Si alloy and Si supersaturation and heterogeneous nucleation, which is driven by the Gibbs free energy difference between *a*-Si:H and *c*-Si phases (denoted as $G_{a\mathrm{Si}}$ and $G_{c\mathrm{Si}}$, respectively); (ii) the droplet dewets the substrate surface at its rear side (low γ^+ surface), thereby a wettability gradient is built up between the front and rear edges of the droplet; (iii) the wettability gradient activates the In droplet flowing towards the *a*-Si:H coated area, which in consequence maintains the contact between the droplet and *a*-Si:H and enables a continuous NW growth.

4. Conclusion

To summarize, we have performed an *in situ* TEM study of in-plane Si NW growth led by a self-propelled In droplet. Geometric analysis unveils a stronger droplet wetting behavior on *a*-Si:H coated SiN_x membrane substrate than on a bare substrate. *In situ* TEM observations, reveal drastic deformations of self-propelling In droplets and their wetting layers at the

advancing edges, which demonstrates a reactive wetting behavior. The droplet movement was powered by a substrate surface wettability gradient established between the front and the rear side of the droplet, which enables progressive Si phase transition and a continuous NW growth. Random turning of the migrating droplet led to a zigzag growth of NWs, probably due to the heterogeneity of *a*-Si:H. Moreover, we observed a growth of faceted *c*-Si nanoflakes rather than NW when the droplet crept slowly (20 nm s^{-1}), whose morphology was transferred from the elongated and faceted droplet-NW contact line. The suppression of this irregular growth was enabled at a high growth rate (100 nm s^{-1}) by increasing the temperature, since higher temperature enables the Si nucleation from In droplet in a lower supersaturation degree, which does not demand drastic droplet reactive wetting to accommodate more Si atoms. Our work provides deep insight into self-propelled droplet transport for yielding low dimensional nanomaterials, which is expected as a promising platform for applications in electronics, photonics, biotechnologies, etc.

Acknowledgements

This work was partly supported by the French RENATECH network and the French National Research Agency (ANR) through the TEMPOS Equipex project (ANR-10-EQPX-0050), poles NanoMAX and NanoTEM. Z.F. thanks the Chinese Scholarship Council and FX-conseil for funding his PhD. Z.F. thanks N.Z. for supporting his PhD.

References

[1] Q. Zhao, H. Cui, Y. Wang, X. Du, Microfluidic Platforms toward Rational Material Fabrication for Biomedical Applications, Small, (2019) e1903798.

[2] L. Feng, S. Li, Y. Li, H. Li, L. Zhang, J. Zhai, Y. Song, B. Liu, L. Jiang, D. Zhu, Super-Hydrophobic Surfaces: From Natural to Artificial, Advanced Materials, 14 (2002) 1857-1860.

[3] J. Hong, J.B. Edel, A.J. deMello, Micro- and nanofluidic systems for high-throughput biological screening, Drug Discov Today, 14 (2009) 134-146.

[4] M. Prakash, D. Quéré, J.W.M. Bush, Surface Tension Transport of Prey by Feeding Shorebirds: The Capillary Ratchet, Science, 320 (2008) 931-934.

[5] O. Gokce, S. Castonguay, Y. Temiz, T. Gervais, E. Delamarche, Self-coalescing flows in microfluidics for pulse-shaped delivery of reagents, Nature, 574 (2019) 228-232.

[6] M. Abdelgawad, A.R. Wheeler, The Digital Revolution: A New Paradigm for Microfluidics, Advanced Materials, 21 (2009) 920-925.

[7] C. Liu, J. Sun, Y. Zhuang, J. Wei, J. Li, L. Dong, D. Yan, A. Hu, X. Zhou, Z. Wang, Self-propelled droplet-based electricity generation, Nanoscale, 10 (2018) 23164-23169.

[8] Y. Zheng, H. Bai, Z. Huang, X. Tian, F.-Q. Nie, Y. Zhao, J. Zhai, L. Jiang, Directional water collection on wetted spider silk, Nature, 463 (2010) 640-643.

[9] Y. Zhao, H. Wang, H. Zhou, T. Lin, Directional Fluid Transport in Thin Porous Materials and its Functional Applications, Small, 13 (2017).

[10] L.I. Segerink, J.C. Eijkel, Nanofluidics in point of care applications, Lab Chip, 14 (2014) 3201-3205.

[11] R.S. Wagner, W.C. Ellis, VAPOR-LIQUID-SOLID MECHANISM OF SINGLE CRYSTAL GROWTH, Applied Physics Letters, 4 (1964) 89-90.

[12] S. Li, Y.-C. Lin, W. Zhao, J. Wu, Z. Wang, Z. Hu, Y. Shen, D.-M. Tang, J. Wang, Q. Zhang, H. Zhu, L. Chu, W. Zhao, C. Liu, Z. Sun, T. Taniguchi, M. Osada, W. Chen, Q.-H. Xu, A.T.S. Wee, K. Suenaga, F. Ding, G. Eda, Vapour–liquid–solid growth of monolayer MoS2 nanoribbons, Nature Materials, 17 (2018) 535-542.

[13] N.P. Dasgupta, J. Sun, C. Liu, S. Brittman, S.C. Andrews, J. Lim, H. Gao, R. Yan, P. Yang, 25th Anniversary Article: Semiconductor Nanowires – Synthesis, Characterization, and Applications, Advanced Materials, 26 (2014) 2137-2184.

[14] D. Jariwala, T.J. Marks, M.C. Hersam, Mixed-dimensional van der Waals heterostructures, Nature Materials, 16 (2017) 170-181.

[15] A. Ismach, D. Kantorovich, E. Joselevich, Carbon Nanotube Graphoepitaxy: Highly Oriented Growth by Faceted Nanosteps, Journal of the American Chemical Society, 127 (2005) 11554-11555.

[16] S.J. Rathi, D.J. Smith, J. Drucker, Guided VLS Growth of Epitaxial Lateral Si Nanowires, Nano Letters, 13 (2013) 3878-3883.

[17] S.A. Fortuna, J. Wen, I.S. Chun, X. Li, Planar GaAs Nanowires on GaAs (100) Substrates: Self-Aligned, Nearly Twin-Defect Free, and Transfer-Printable, Nano Letters, 8 (2008) 4421-4427.

[18] D. Tsivion, M. Schvartzman, R. Popovitz-Biro, P. von Huth, E. Joselevich, Guided Growth of Millimeter-Long Horizontal Nanowires with Controlled Orientations, Science, 333 (2011) 1003-1007.

[19] L. Yu, W. Chen, B. O'Donnell, G. Patriarche, S. Bouchoule, P. Pareige, R. Rogel, A.C. Salaun, L. Pichon, P. Roca i Cabarrocas, Growth-in-place deployment of in-plane silicon nanowires, Applied Physics Letters, 99 (2011) 203104-203103.

[20] Y. Zhao, H. Ma, T. Dong, J. Wang, L. Yu, J. Xu, Y. Shi, K. Chen, P. Roca i Cabarrocas, Nanodroplet Hydrodynamic Transformation of Uniform Amorphous Bilayer into Highly Modulated Ge/Si Island-Chains, Nano Letters, 18 (2018) 6931-6940.

[21] Y. Shan, S.J. Fonash, Self-Assembling Silicon Nanowires for Device Applications Using the Nanochannel-Guided "Grow-in-Place" Approach, ACS Nano, 2 (2008) 429-434.

[22] E. Mataev, S.K. Rastogi, A. Madhusudan, J. Bone, N. Lamprinakos, Y. Picard, T. Cohen-Karni, Synthesis of Group IV Nanowires on Graphene: The Case of Ge Nanocrawlers, Nano Letters, 16 (2016) 5267-5272.

[23] L.C. Campos, V.R. Manfrinato, J.D. Sanchez-Yamagishi, J. Kong, P. Jarillo-Herrero, Anisotropic Etching and Nanoribbon Formation in Single-Layer Graphene, Nano Letters, 9 (2009) 2600-2604.

[24] F. Brochard, Motions of droplets on solid surfaces induced by chemical or thermal gradients, Langmuir, 5 (1989) 432-438.

[25] P.G. de Gennes, The dynamics of reactive wetting on solid surfaces, Physica A: Statistical Mechanics and its Applications, 249 (1998) 196-205.

[26] M.K. Chaudhury, G.M. Whitesides, How to Make Water Run Uphill, Science, 256 (1992) 1539-1541.

[27] F.D. Dos Santos, T. Ondarçuhu, Free-Running Droplets, Physical Review Letters, 75 (1995) 2972-2975.

[28] A.K. Schmid, N.C. Bartelt, R.Q. Hwang, Alloying at Surfaces by the Migration of Reactive Two-Dimensional Islands, Science, 290 (2000) 1561-1564.

[29] K. Ichimura, S.-K. Oh, M. Nakagawa, Light-Driven Motion of Liquids on a Photoresponsive Surface, Science, 288 (2000) 1624-1626.

[30] Q. Sun, D. Wang, Y. Li, J. Zhang, S. Ye, J. Cui, L. Chen, Z. Wang, H.J. Butt, D. Vollmer, X. Deng, Surface charge printing for programmed droplet transport, Nat Mater, 18 (2019) 936-941.

[31] M.R. Frances, Controlling nanowire structures through real time growth studies, Reports on Progress in Physics, 73 (2010) 114501.

[32] J.-C. Harmand, G. Patriarche, F. Glas, F. Panciera, I. Florea, J.-L. Maurice, L. Travers, Y. Ollivier, Atomic Step Flow on a Nanofacet, Physical Review Letters, 121 (2018) 166101.

[33] R. Boston, Z. Schnepp, Y. Nemoto, Y. Sakka, S.R. Hall, In Situ TEM Observation of a Microcrucible Mechanism of Nanowire Growth, Science, 344 (2014) 623-626.

[34] B.J. Kim, J. Tersoff, S. Kodambaka, M.C. Reuter, E.A. Stach, F.M. Ross, Kinetics of Individual Nucleation Events Observed in Nanoscale Vapor-Liquid-Solid Growth, Science, 322 (2008) 1070-1073.

[35] D. Jacobsson, F. Panciera, J. Tersoff, M.C. Reuter, S. Lehmann, S. Hofmann, K.A. Dick, F.M. Ross, Interface dynamics and crystal phase switching in GaAs nanowires, Nature, 531 (2016) 317-322.

[36] J.B. Hannon, S. Kodambaka, F.M. Ross, R.M. Tromp, The influence of the surface migration of gold on the growth of silicon nanowires, Nature, 440 (2006) 69-71.

[37] Y.-C. Chou, K. Hillerich, J. Tersoff, M.C. Reuter, K.A. Dick, F.M. Ross, Atomic-Scale Variability and Control of III-V Nanowire Growth Kinetics, Science, 343 (2014) 281-284.

[38] Y. Jiang, Z. Zhang, W. Yuan, X. Zhang, Y. Wang, Z. Zhang, Recent advances in gas-involved in situ studies via transmission electron microscopy, Nano Research, 11 (2018) 42-67.

[39] L. Yu, P.-J. Alet, G. Picardi, P. Roca i Cabarrocas, An In-Plane Solid-Liquid-Solid Growth Mode for Self-Avoiding Lateral Silicon Nanowires, Physical Review Letters, 102 (2009) 125501.

[40] L. Yu, P.R. i Cabarrocas, Growth mechanism and dynamics of in-plane solid-liquid-solid silicon nanowires, Physical Review B, 81 (2010) 085323.

[41] G. Rohrer, Grain boundary energy anisotropy: a review, Journal of Materials Science, 46 (2011) 5881-5895.

[42] R.J. Jaccodine, Surface Energy of Germanium and Silicon, Journal of The Electrochemical Society, 110 (1963) 524-527.

[43] B. Pignataro, G. Grasso, L. Renna, G. Marletta, Adhesion properties on nanometric scale of silicon oxide and silicon nitride surfaces modified by 1-octadecene, Surface and Interface Analysis, 33 (2002) 54-58.

[44] D.W.G. White, The surface tensions of indium and cadmium, Metallurgical Transactions, 3 (1972) 1933-1936.

[45] R. Boistelle, J.P. Astier, Crystallization mechanisms in solution, Journal of Crystal Growth, 90 (1988) 17.

[46] R. Cupryś, B. Major, W. Wołczyński, Transition of flake into fibre structure in eutectic Al-Si, Mater. Sci. Forum, 329 (2000) 161-166.

[47] H.K. Yu, J.-L. Lee, Growth mechanism of metal-oxide nanowires synthesized by electron beam evaporation: A self-catalytic vapor-liquid-solid process, Sci. Rep., 4 (2014).

[48] P. Roura, F. Taïr, J. Farjas, P.R.i. Cabarrocas, Measurement of the specific heat and determination of the thermodynamic functions of relaxed amorphous silicon, Journal of Applied Physics, 113 (2013) 173515.

[49] E. Azrak, W. Chen, S. Moldovan, S. Gao, S. Duguay, P. Pareige, P. Roca i Cabarrocas, Growth of In-Plane Ge1–xSnx Nanowires with 22 at. % Sn Using a Solid–Liquid–Solid Mechanism, The Journal of Physical Chemistry C, 122 (2018) 26236-26242.

[50] Z. Xue, M. Xu, X. Li, J. Wang, X. Jiang, X. Wei, L. Yu, Q. Chen, J. Wang, J. Xu, Y. Shi, K. Chen, P. Roca i Cabarrocas, In-Plane Self-Turning and Twin Dynamics Renders Large Stretchability to Mono-Like Zigzag Silicon Nanowire Springs, Advanced Functional Materials, 26 (2016) 5352-5359.

[51] J.M. Rallison, The Deformation of Small Viscous Drops and Bubbles in Shear Flows, Annual Review of Fluid Mechanics, 16 (1984) 45-66.

[52] H.A. Stone, Dynamics of Drop Deformation and Breakup in Viscous Fluids, Annual Review of Fluid Mechanics, 26 (1994) 65-102.

[53] R.W. Olesinski, N. Kanani, G.J. Abbaschian, The In-Si (Indium-Silicon) system, Bulletin of Alloy Phase Diagrams, 6 (1985) 128-130.

[54] R.W. Olesinski, G.J. Abbaschian, The Si-Sn (Silicon-Tin) system, Bulletin of Alloy Phase Diagrams, 5 (1984) 273-276.

[55] R.W. Olesinski, G.J. Abbaschian, The Ge-Sn (Germanium-Tin) system, Bulletin of Alloy Phase Diagrams, 5 (1984) 265-271.

[56] P. Atkins, J. de Paula, J. Keeler, Physical Chemistry, Oxford Press 2018, 11th Edition.

[57] S. Kodambaka, J.B. Hannon, R.M. Tromp, F.M. Ross, Control of Si Nanowire Growth by Oxygen, Nano Letters, 6 (2006) 1292-1296.

[58] S. Misra, L. Yu, W. Chen, P. Roca i Cabarrocas, Wetting Layer: The Key Player in Plasma-Assisted Silicon Nanowire Growth Mediated by Tin, The Journal of Physical Chemistry C, 117 (2013) 17786-17790.

[59] M.S. Seifner, A. Dijkstra, J. Bernardi, A. Steiger-Thirsfeld, M. Sistani, A. Lugstein, J.E.M. Haverkort, S. Barth, Epitaxial $Ge_{0.81}Sn_{0.19}$ Nanowires for Nanoscale Mid-Infrared Emitters, ACS Nano, 13 (2019) 8047-8054.

[60] K.W. Schwarz, J. Tersoff, Elementary Processes in Nanowire Growth, Nano Letters, 11 (2011) 316-320.